Microelectronics Journal 44 (2013) 1175–1192

Contents lists available at ScienceDirect

Microelectronics Journal

journal homepage: www.elsevier.com/locate/mejo

High frequency flipped voltage follower with improved performance and its application

Urvashi Singh, Maneesha Gupta*

Electronics & Communication Engineering Department, NSIT, New Delhi, India

ARTICLE INFO

Article history:
Received 25 April 2012
Received in revised form
30 July 2013
Accepted 5 August 2013
Available online 10 September 2013

Keywords:
Flipped voltage follower
Bandwidth extension ratio
Inductive peaking
Small-signal model
Mixed-signal circuits

ABSTRACT

In this paper a wideband flipped voltage follower (FVF) with low output impedance at high frequency has been proposed. Inductive-peaking-based bandwidth extension technique is employed in the FVF cell. The small signal high-frequency analysis of both conventional and proposed FVF has been done. It is shown in analytical derivation of the proposed FVF that by adding an inductive element in the feedback path, the bandwidth is enhanced. Simulation results show that bandwidth extension ratio (BWER) of proposed FVF is about 2.00, without extra dc power dissipation. A wideband low voltage current mirror has been developed by using proposed FVF in place of conventional FVF and by doing so, BWER of 2.98 has been achieved. The performances of circuits are verified in TSMC 0.18 μm CMOS, BSIM3 and Level 49 technology with 1.5 V power supply and by using Spectre simulator of Cadence.

1. Introduction

One of the widely used building blocks in analog and mixed-signal circuits is voltage follower [1]. The modern deep submicron CMOS technologies have forced the researchers to design, low power high speed MOS voltage buffers. Moreover, the growth in portable electronic devices imposes stringent requirements of low-voltage operation and fast settling response on these buffers.

Carvajal et al. [2] have introduced a voltage buffer, with high slew-rate and low static power consumption, known as flipped voltage follower (FVF). A FVF cell can operate at low supply voltage and has almost unity gain (on neglecting the short-channel effects). It has been shown in [2] that, a FVF cell has better performance than that of conventional voltage followers.

Due to its almost ideal voltage buffer performance, FVF has replaced the conventional voltage buffers in many circuits. The designers have used FVF in current sensor, current mirrors, differential pair, OTA, instrumentation amplifier, arithmetic circuits, translinear loops and many more low-voltage and/or low-power applications [2–7].

Recently several modifications of FVF are proposed to increase the signal swing and to reduce both supply voltage requirements and output impedance [8–10]. Due to the explosive growth of multimedia communication systems, the demand of wideband voltage follower has tremendously increased in many design topologies. But the area of bandwidth enhancement of FVF has not been much explored till date, to the best of our knowledge. This paper focuses on the bandwidth enhancement of the conventional FVF.

There are various techniques available to increase the bandwidth of a circuit: resistive compensation technique [11], capacitive compensation technique [12], feedforward compensation technique [13] and inductive peaking technique [14]. In this paper we have used inductive peaking technique to increase the bandwidth of the conventional FVF.

Usually obtaining the wider bandwidth tends to require higher power dissipation for a given technology [15]. By using inductive-peaking technique, the bandwidth of a circuit can be enhanced, without additional dc power dissipation [16]. Also, on comparison with resistive compensation technique, inductive-peaking technique can provide bandwidth extension without deteriorating the noise performance of the circuit [17]. Thus the proposed wideband FVF is suitable for low voltage high-speed operation.

In the work, we have introduced the proposed high frequency FVF cell in a low voltage current mirror [18] for performance improvement. The analytical formulation of transfer function of the conventional FVF is given in Section 2. The small-signal analysis and the output impedance of the proposed FVF are derived in Section 3. Section 4 proposes a low voltage current mirror, whose bandwidth is

* Corresponding author. Tel.: +91 981 075 3962; fax: +91 112 509 9022.
E-mail address: maneeshapub@gmail.com (M. Gupta).

0026-2692/$ - see front matter © 2013 Elsevier Ltd. All rights reserved.
http://dx.doi.org/10.1016/j.mejo.2013.08.002

enhanced by using the FVF discussed in Section 3. The simulation results of all designed circuits are given in Section 5. Finally conclusions have been drawn in Section 6.

2. Transfer function and output impedance of the conventional FVF

The conventional FVF circuit and its small signal equivalent model are shown in Figs. 1 and 2 respectively. To neglect the substrate-bias effect and to simplify the transfer function derivation, it has been assumed that source of nMOS transistor is connected to its substrate and simulations are also performed on the basis of same assumption [5].

In the analysis r_{o1} and r_{o2} are the resistances due to channel length modulation effect, C_{gs1} and C_{gs2} are the gate to source capacitances, g_{m1} and g_{m2} are the transconductances of transistors M1 and M2 respectively. R_b is the output impedance of the current source and v_{gs2} stands for gate to source voltage of M2.

On applying KCL at nodes (a) and (b) in the small signal model of the conventional FVF (Fig. 2), we get

$$sC_{gs1}(v_{out}-v_{in})+g_{m2}v_{gs2}-g_{m1}(v_{in}-v_{out})+\frac{(v_{out}-v_{gs2})}{r_{o1}}+\frac{v_{out}}{r_{o2}}=0 \tag{1}$$

$$\frac{(v_{gs2}-v_{out})}{r_{o1}}+sC_{gs2}v_{gs2}+\frac{v_{gs2}}{R_b}+g_{m1}(v_{in}-v_{out})=0 \tag{2}$$

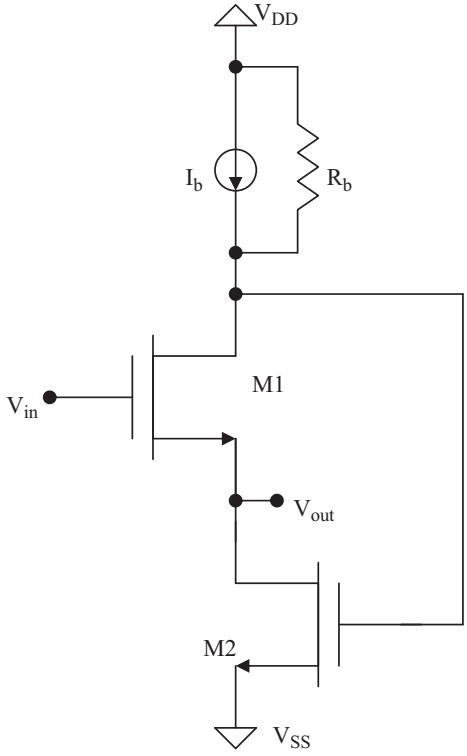

Fig. 1. Conventional FVF.

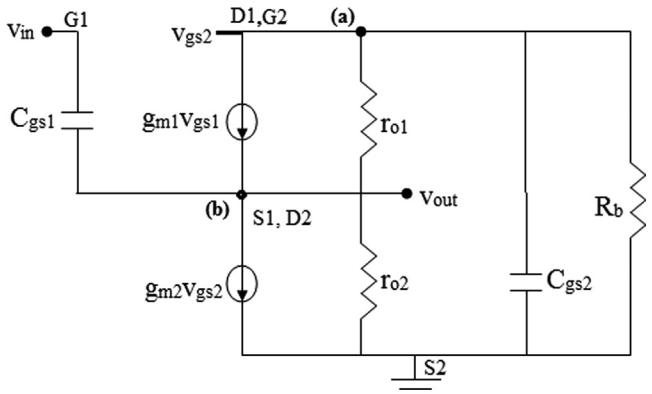

Fig. 2. Small-signal equivalent model of conventional FVF.

Using Eqs. (1) and (2), the obtained voltage gain $A_v(s)$ of the conventional FVF is

$$A_v(s)=\frac{(s^2C_{gs1}C_{gs2}r_{o1}{}^2r_{o2}R_b+sr_{o1}r_{o2}\{C_{gs1}(R_b+r_{o1})+C_{gs2}g_{m1}r_{o1}R_b\}+g_{m1}g_{m2}r_{o1}{}^2r_{o2}R_b+g_{m1}r_{o1}{}^2r_{o2})}{\left(\begin{array}{l}s^2C_{gs1}C_{gs2}r_{o1}{}^2r_{o2}R_b+sr_{o1}\{C_{gs1}r_{o2}(R_b+r_{o1})+C_{gs2}R_b(r_{o1}+r_{o2})+C_{gs2}g_{m1}r_{o1}r_{o2}R_b\}+g_{m1}g_{m2}r_{o1}{}^2r_{o2}R_b+\\ g_{m1}r_{o1}{}^2r_{o2}+g_{m2}r_{o1}r_{o2}R_b+r_{o1}R_b+r_{o1}(r_{o1}+r_{o2})\end{array}\right)} \tag{3}$$

Assuming $r_{o1}=r_{o2}=r_o$ and $C_{gs1}=C_{gs2}=C_{gs}$ in Eq. (3), we get

$$A_v(s)=\frac{s^2+s\{((R_b+r_o)/C_{gs}r_oR_b)+(g_{m1}/C_{gs})\}+(g_{m1}g_{m2}/C_{gs}^2)+(g_{m1}/C_{gs}^2R_b)}{s^2+s\{(R_b+r_o)/C_{gs}r_oR_b+(2/C_{gs}r_o)+(g_{m1}/C_{gs})\}+(g_{m1}g_{m2}/C_{gs}^2)+(g_{m2}/C_{gs}^2r_o)+(g_{m1}/C_{gs}^2R_b)+(R_b+2r_o/C_{gs}^2r_o^2R_b)}. \tag{4}$$

Using the assumptions $g_{mx}R_b\gg1$ and $g_{mx}r_o\gg1$ (where,$x=1,2$) in Eq. (4) then, the transfer function is reduced to

$$A_v(s)=\frac{s^2+s\{(R_b+r_o)/C_{gs}r_oR_b+(g_{m1}/C_{gs})\}+(g_{m1}g_{m2}/C_{gs}{}^2)}{s^2+s\{(R_b+r_o)/C_{gs}r_oR_b+(g_{m1}/C_{gs})\}+(g_{m1}g_{m2}/C_{gs}{}^2)+(R_b+2r_o/C_{gs}{}^2r_o{}^2R_b)} \tag{5}$$

Also

$$\frac{(R_b+r_o)}{C_{gs}r_oR_b}+\left(\frac{g_{m1}}{C_{gs}}\right)=\frac{R_b+r_o+g_{m1}r_oR_b}{C_{gs}r_oR_b}\cong\left(\frac{g_{m1}}{C_{gs}}\right) \tag{6}$$

Finally

$$A_v(s)=\frac{s^2+s(g_{m1}/C_{gs})+(g_{m1}g_{m2}/C_{gs}^2)}{s^2+s(g_{m1}/C_{gs})+(g_{m1}g_{m2}/C_{gs}^2)+\left(R_b+2r_o/C_{gs}^2r_o{}^2R_b\right)} \tag{7}$$

It can be expressed as

$$A_v(s)=\frac{s^2+a_1s+a_2}{s^2+a_1s+(a_2+\Delta a_2)} \tag{8}$$

where, $a_1=(g_{m1}/C_{gs})$, $a_2=(g_{m1}g_{m2}/C_{gs}{}^2)$ and $\Delta a_2=\{(R_b+2r_o)/C_{gs}{}^2r_o{}^2R_b\}$

From Eq. (8), the zeros and poles of the conventional FVF are found to be

$$Z_{1,2}=\frac{-a_1}{2}\left[1\mp\sqrt{1-4\left(\frac{a_2}{a_1^2}\right)}\right] \tag{9}$$

$$P_{1,2}=\frac{-a_1}{2}\left[1\mp\sqrt{1-4\left(\frac{(a_2+\Delta a_2)}{a_1^2}\right)}\right] \tag{10}$$

By definition [19], at $\omega=\omega_o$,

$$|A_v(\omega_0)|^2=0.5|A_v(0)|^2 \tag{11}$$

where $|A_v(0)|^2=1$ of a voltage buffer.

From Eqs. (7) and (11), the -3 dB frequency is given by

$$\omega_o=\sqrt{\left\{\left(\frac{2g_{m1}g_{m2}}{C_{gs}^2}\right)-\left(\frac{g_{m1}}{C_{gs}}\right)^2-2\left(\frac{R_b+2r_o}{C_{gs}^2r_o^2R_b}\right)\right\}} \tag{12}$$

It is shown in [2] that, the output impedance of the conventional FVF is

$$Z_{OUT}=\frac{1}{g_{m1}g_{m2}r_o} \tag{13}$$

In this work, the conventional FVF cell is modified to achieve extremely large bandwidth and very low output impedance at high frequency by using an inductive element in the feedback path, which will be discussed and analyzed in the next section.

3. Proposed wideband and high performance FVF

In this section we have modified the conventional FVF by adding an inductive element (Z) in the feedback path between drain terminal of M1 and gate terminal of M2 (as shown in Fig. 3). On insertion of Z in the feedback path, the impedance of the path increases and thus it directs the current to flow into the output node (which is a low impedance path) at high frequency. This increased current is available to charge-up the output parasitic and load capacitances and thus reduces the rise-time at the output node [20]. The small-signal model of the proposed FVF is shown in Fig. 4.

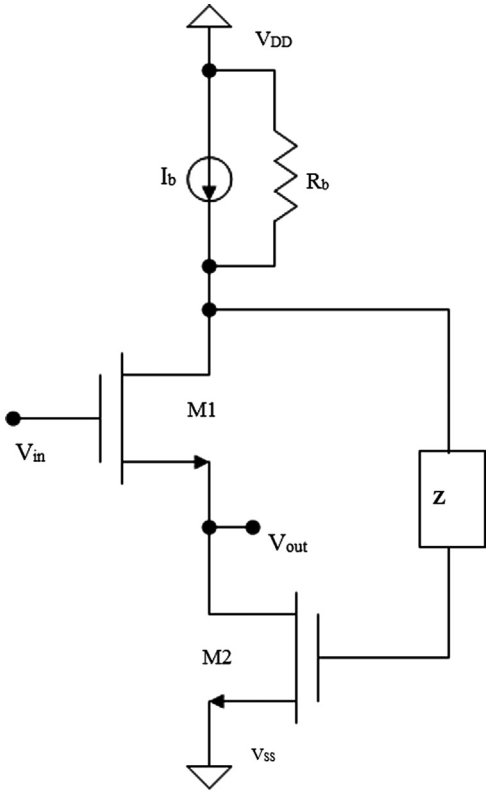

Fig. 3. Proposed FVF.

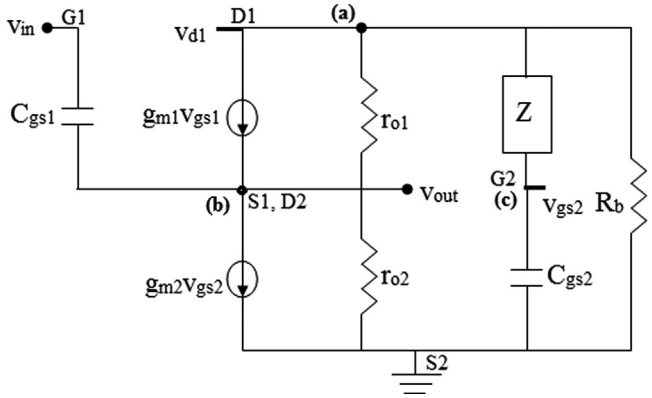

Fig. 4. Small-signal equivalent model of proposed FVF.

3.1. High frequency analysis of the proposed FVF

In the analysis the resistive or inductive element is denoted by Z which is employed in the feedback path of the FVF and v_{d1} is the voltage drop at the drain terminal of MOS transistor M1. On applying the KCL at nodes (a), (b) and (c) in the small-signal model, we get

$$sC_{gs1}(v_{out}-v_{in})+g_{m2}v_{gs2}-g_{m1}(v_{in}-v_{out})+\frac{(v_{out}-v_{d1})}{r_{o1}}+\frac{v_{out}}{r_{o2}}=0 \tag{14}$$

$$\frac{(v_{d1}-v_{out})}{r_{o1}}+\frac{(v_{d1}-v_{gs2})}{Z}+\frac{v_{d1}}{R_b}+g_{m1}(v_{in}-v_{out})=0 \tag{15}$$

$$\frac{(v_{gs2}-v_{d1})}{Z}+sC_{gs2}v_{gs2}=0 \tag{16}$$

By using Eqs. (14)–(16), the transfer function of the proposed FVF is found to be

$$A_v(s)=\frac{\left(\begin{array}{l}s^2C_{gs1}C_{gs2}r_{o1}r_{o2}\{Z(R_b+r_{o1})+R_br_{o1}\}+sr_{o1}r_{o2}\{C_{gs1}(R_b+r_{o1})+C_{gs2}g_{m1}r_{o1}(R_b+Z)\}\\+g_{m1}g_{m2}{r_{o1}}^2r_{o2}R_b+g_{m1}{r_{o1}}^2r_{o2}\end{array}\right)}{\left(\begin{array}{l}s^2C_{gs1}C_{gs2}r_{o1}r_{o2}\{Z(R_b+r_{o1})+R_br_{o1}\}+sr_{o1}\{C_{gs1}r_{o2}(R_b+r_{o1})+C_{gs2}g_{m1}r_{o1}r_{o2}(R_b+Z)+C_{gs2}ZR_b\}+\\g_{m1}g_{m2}{r_{o1}}^2r_{o2}R_b+g_{m1}{r_{o1}}^2r_{o2}+g_{m2}r_{o1}r_{o2}R_b\end{array}\right)} \tag{17}$$

From Eq. (17) it can be observed that, the addition of a Z element in the feedback path of the FVF modifies the transfer function. This modification depends upon the type of chosen element (Z).

In the paper, we have enhanced the bandwidth of the FVF by adding (i) an inductor and (ii) a series combination of a resistor and an inductor in the feedback path.

3.1.1. *Modification by adding an inductor in the feedback path*

If Z is an inductor (sL) then, the Eq. (17) transforms into

$$A_v(s)=\frac{\left(\begin{array}{l}s^3r_{o1}r_{o2}C_{gs1}C_{gs2}L(R_b+r_{o1})+s^2r_{o1}^2r_{o2}C_{gs2}(C_{gs1}R_b+g_{m1}L)+\\sr_{o1}r_{o2}\{C_{gs1}(R_b+r_{o1})+g_{m1}r_{o1}C_{gs2}R_b\}+g_{m1}r_{o1}^2r_{o2}+g_{m1}g_{m2}r_{o1}^2r_{o2}R_b\end{array}\right)}{\left(\begin{array}{l}s^3r_{o1}r_{o2}C_{gs1}C_{gs2}L(R_b+r_{o1})+s^2r_{o1}C_{gs2}\{r_{o1}r_{o2}C_{gs1}R_b+L(r_{o1}+r_{o2}+R_b)+g_{m1}r_{o1}r_{o2}L\}+\\sr_{o1}\{r_{o2}C_{gs1}(R_b+r_{o1})+C_{gs2}R_b(r_{o1}+r_{o2})+g_{m1}r_{o1}r_{o2}C_{gs2}R_b\}+\\g_{m1}r_{o1}^2r_{o2}+g_{m2}r_{o1}r_{o2}R_b+g_{m1}g_{m2}r_{o1}^2r_{o2}R_b+r_{o1}(r_{o1}+r_{o2}+R_b)\end{array}\right)} \tag{18}$$

Note that, the added inductor has no effect on the DC characteristics. The modified FVF has a third-order transfer function. The effect of using an inductor in feedback path is to transform 2nd order transfer function into 3rd order (i.e. it adds a zero and a pole to the transfer function), which allows more control over the frequency response of the FVF [21]. With the assumptions $r_{o1}=r_{o2}=r_o$ and $C_{gs1}=C_{gs2}=C_{gs}$, the transfer function is simplified into

$$A_v(s)\approx\frac{(s^2r_o^3C_{gs}(C_{gs}R_b+g_{m1}L)+sr_o{}^2C_{gs}\{(R_b+r_o)+g_{m1}r_oR_b\}+g_{m1}r_o^3+g_{m1}g_{m2}r_o^3R_b)}{\left(\begin{array}{l}s^2r_oC_{gs}\{r_o{}^2C_{gs}R_b+L(2r_o+R_b)+g_{m1}r_o^2L\}+sr_o^2C_{gs}\{r_o+3R_b+g_{m1}r_oR_b\}+\\g_{m1}r_o^3+g_{m2}r_o^2R_b+g_{m1}g_{m2}r_o^3R_b+r_o(2r_o+R_b)\end{array}\right)} \tag{19}$$

Since $(2r_o+R_b)<g_{m1}r_o^2$, hence Eq. (19) is transformed into

$$A_v(s)\approx\frac{s^2+s\{(R_b+r_o+g_{m1}r_oR_b)/r_o(C_{gs}R_b+g_{m1}L)\}+(g_{m1}g_{m2}R_b/C_{gs}(C_{gs}R_b+g_{m1}L))}{\left(\begin{array}{l}s^2+s\{(3R_b+r_o+g_{m1}r_oR_b)/r_o(C_{gs}R_b+g_{m1}L)\}\\+(g_{m1}g_{m2}R_b/C_{gs}(C_{gs}R_b+g_{m1}L))+(2r_o+R_b/r_o{}^2C_{gs}(C_{gs}R_b+g_{m1}L))\end{array}\right)} \tag{20}$$

The transfer function of the proposed FVF can be expressed as

$$A_v(s)=\frac{s^2+b_1s+b_0}{s^2+(b_1+\Delta b_1)s+(b_0+\Delta b_0)} \tag{21}$$

where

$$b_1=\left(\frac{(R_b+r_o+g_{m1}r_oR_b)}{r_o(C_{gs}R_b+g_{m1}L)}\right),\Delta b_1=\left(\frac{2R_b}{r_o(C_{gs}R_b+g_{m1}L)}\right)$$

$$b_0=\left(\frac{g_{m1}g_{m2}R_b}{C_{gs}(C_{gs}R_b+g_{m1}L)}\right)\text{ and }\Delta b_0=\left(\frac{2r_o+R_b}{r_o{}^2C_{gs}(C_{gs}R_b+g_{m1}L)}\right)$$

From Eq. (21) the zeros and poles of the modified FVF are found to be

$$Z_{1,2}=\frac{-b_1}{2}\left[1\mp\sqrt{1-4\left(\frac{b_0}{b_1{}^2}\right)}\right] \tag{22}$$

$$P_{1,2}=\frac{-(b_1+\Delta b_1)}{2}\left[1\mp\sqrt{1-4\left(\frac{(b_0+\Delta b_0)}{(b_1+\Delta b_1)^2}\right)}\right] \tag{23}$$

From Eqs. (11) and (20) the -3 dB frequency is given by

$$\omega_0=\sqrt{\left\{\begin{array}{l}2\left(\frac{g_{m1}g_{m2}R_b}{C_{gs}(C_{gs}R_b+g_{m1}L)}\right)-2\left(\frac{2r_o+R_b}{r_o{}^2C_{gs}(C_{gs}R_b+g_{m1}L)}\right)-\left(\frac{(R_b+r_o+g_{m1}r_oR_b)}{r_o(C_{gs}R_b+g_{m1}L)}\right)^2+\left(\frac{2R_b}{r_o(C_{gs}R_b+g_{m1}L)}\right)^2+\\4\left(\frac{R_b(R_b+r_o+g_{m1}r_oR_b)}{r_o{}^2(C_{gs}R_b+g_{m1}L)}\right)\end{array}\right\}} \tag{24}$$

3.1.2. Modification by adding a series combination of an inductor and a resistor in the feedback path

If Z ($=R+sL$) is a series combination of an inductor (sL) and a resistor (R), the transfer function of the improved FVF is given by

$$A_v(s)=\frac{\left(\begin{array}{l}s^2C_{gs1}C_{gs2}r_{o1}r_{o2}\{(sL+R)(R_b+r_{o1})+R_br_{o1}\}+sr_{o1}r_{o2}\{C_{gs1}(R_b+r_{o1})+C_{gs2}g_{m1}r_{o1}(R_b+R+sL)\}\\+g_{m1}g_{m2}{r_{o1}}^2r_{o2}R_b+g_{m1}{r_{o1}}^2r_{o2}\end{array}\right)}{\left(\begin{array}{l}s^2C_{gs1}C_{gs2}r_{o1}r_{o2}\{(sL+R)(R_b+r_{o1})+R_br_{o1}\}+sr_{o1}\{C_{gs1}r_{o2}(R_b+r_{o1})+C_{gs2}g_{m1}r_{o1}r_{o2}(R_b+R+sL)+C_{gs2}R_b(sL+R)\}\\+g_{m1}g_{m2}{r_{o1}}^2r_{o2}R_b+g_{m1}{r_{o1}}^2r_{o2}+g_{m2}r_{o1}r_{o2}R_b\end{array}\right)} \tag{25}$$

Using assumptions $r_{o1}=r_{o2}=r_o$ and $C_{gs1}=C_{gs2}=C_{gs}$ and simplifying the transfer function, we get

$$A_v(s)=\frac{\left(\begin{array}{l}s^3r_o^2{C_{gs}}^2L(R_b+r_o)+s^2r_o^2C_{gs}\{C_{gs}\{R(R_b+r_o)+R_br_o\}+g_{m1}r_oL\}+\\sr_o^2C_{gs}\{R_b+r_o+g_{m1}r_o(R_b+R)\}+g_{m1}g_{m2}r_o^3R_b\end{array}\right)}{\left(\begin{array}{l}s^3r_o^2C_{gs}^2L(R_b+r_o)+s^2r_oC_{gs}\{r_oC_{gs}(R(R_b+r_o)+R_br_o)+LR_b+g_{m1}r_o^2L\}+\\sr_oC_{gs}\{r_o(R_b+r_o)+R_bR+g_{m1}r_o^2(R+R_b)\}+g_{m1}g_{m2}r_o^3R_b+r_o(2r_o+R_b)\end{array}\right)} \tag{26}$$

Let $R_b<g_{m1}r_o^2$ and performing some simplifications Eq. (26) is transformed into

$$A_v(s)=\frac{\left(\begin{array}{l}s^2+s(R_b+r_o+g_{m1}r_o(R_b+R)/C_{gs}\{R(R_b+r_o)+R_br_o\}\\+g_{m1}r_oL)+(g_{m1}g_{m2}r_oR_b/C_{gs}\{C_{gs}\{R(R_b+r_o)+R_br_o\}+g_{m1}r_oL\})\end{array}\right)}{\left(\begin{array}{l}s^2+s(r_o(R_b+r_o)+R_bR+g_{m1}r_o^2(R+R_b)/r_oC_{gs}(R(R_b+r_o)+R_br_o)+g_{m1}r_o^2L)\\+(g_{m1}g_{m2}r_o^2R_b+2r_o+R_b/r_oC_{gs}\{C_{gs}\{R(R_b+r_o)+R_br_o\}+g_{m1}r_oL\})\end{array}\right)} \tag{27}$$

The transfer function derived in Eq. (27) can be expressed as

$$A_v(s)=\frac{s^2+c_1s+c_0}{s^2+(c_1+\Delta c_1)s+(c_0+\Delta c_0)} \tag{28}$$

where

$$c_1=\left(\frac{R_b+r_o+g_{m1}r_o(R_b+R)}{C_{gs}\{R(R_b+r_o)+R_br_o\}+g_{m1}r_oL}\right)\quad \Delta c_1=\left(\frac{R_bR}{r_oC_{gs}(R(R_b+r_o)+R_br_o)+g_{m1}{r_o}^2L}\right)$$

$$c_0=\left(\frac{g_{m1}g_{m2}r_oR_b}{C_{gs}\{C_{gs}\{R(R_b+r_o)+R_br_o\}+g_{m1}r_oL\}}\right)\text{ and }\Delta c_0=\left(\frac{2r_o+R_b}{r_oC_{gs}\{C_{gs}\{R(R_b+r_o)+R_br_o\}+g_{m1}r_oL\}}\right)$$

From Eq. (28), the zeros and poles of the modified FVF are found to be

$$Z_{1,2}=\frac{-c_1}{2}\left[1\mp\sqrt{1-4\left(\frac{c_0}{{c_1}^2}\right)}\right] \tag{29}$$

$$P_{1,2}=\frac{-(c_1+\Delta c_1)}{2}\left[1\mp\sqrt{1-4\left(\frac{(c_0+\Delta c_0)}{(c_1+\Delta c_1)^2}\right)}\right] \tag{30}$$

From Eqs. (11) and (27), the -3 dB frequency is given by

$$\omega_0=\sqrt{\left\{\begin{array}{l}2\left(\frac{g_{m1}g_{m2}r_o^2R_b-(2r_o+R_b)}{r_oC_{gs}\{C_{gs}\{R(R_b+r_o)+R_br_o\}+g_{m1}r_oL\}}\right)+\\\left(\frac{(R_bR)^2-\{r_o(R_b+r_o)+g_{m1}r_o^2(R_b+R)\}^2+2R_bR(r_o(R_b+r_o)++g_{m1}r_o^2(R+R_b))}{(r_oC_{gs}(R(R_b+r_o)+R_br_o)+g_{m1}{r_o}^2L)^2}\right)\end{array}\right\}} \tag{31}$$

On comparing Eqs. (12), (24) and (31), it can be seen that, there is a very large bandwidth extension by using inductive-peaking technique in the conventional FVF and this extension is obtained without affecting the mid-band gain of the FVF, which can be verified from the transfer function of the modified FVF (Eq. (17)).

To implement the proposed FVF cell, on-chip spiral inductors can be used. However, it should also be noted that, the area efficiency is the main concerned in case of inductive-peaking. The area efficiency can be improved by using multilevel spiral structure technique (as a monolithically implementable structure) [22,23]. Alternatively inductor can be implemented using active device, for which various implementations are available in literature [24–26].

3.1.3. Stability analysis

A FVF cell is a series-shunt negative feedback amplifier. The advantages of negative feedback include: gain desensitization, bandwidth extension, impedance modification, and nonlinearity reduction. The stability of a single-input, single-output, linear time invariant control system can be found by Routh–Hurwitz criterion [27]. The Routh–Hurwitz stability criterion states that the number of roots with positive real parts is equal to the number of changes in sign of the coefficients in the first column of the matrix. By using the coefficients of a denominator polynomial of transfer function one can determine whether the feedback system is stable or not.

The stability of both the proposed FVF with an inductor and with series combination of a resistor and an inductor in feedback path, have been found by the Routh arrays shown in Tables 5 and 6, respectively. It can be seen that the proposed FVF cells have no closed-loop right hand poles. Hence, the proposed FVF cells are stable.

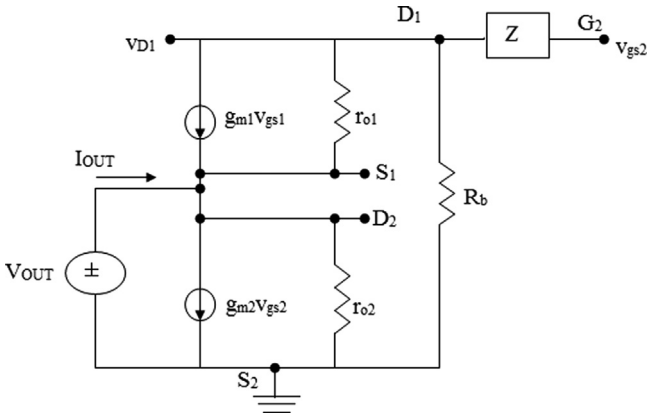

Fig. 5. Small-signal model of the proposed FVF for output impedance calculation.

3.2. Output impedance analysis

Small-signal model of the proposed FVF for output impedance calculation is shown in Fig. 5. To calculate the output impedance a test voltage source is placed at the output node of the proposed FVF as shown in Fig. 5. The relation between the test source and test current will define the output impedance of the modified FVF.

The derived output impedance is given by

$$Z_{OUT} = \frac{r_{o2}R_b}{g_{m1}r_{o1}R_b + g_{m1}g_{m2}r_{o1}r_{o2}(R_b + Z)} \tag{32}$$

On assuming, $r_{o1}=r_{o2}=r_o$, the output impedance becomes

$$Z_{OUT} = \frac{R_b}{g_{m1}R_b + g_{m1}g_{m2}r_o(R_b + Z)} \tag{33}$$

On simplifying Eq. (33) we get

$$Z_{OUT} = \frac{1}{g_{m1}g_{m2}r_o(1 + Z/R_b)} \tag{34}$$

The output impedance of the proposed FVF with inductor (Z=sL) in the feedback path is given by

$$Z_{OUT} = \frac{1}{g_{m1}g_{m2}r_o(1 + sL/R_b)} \tag{35}$$

At $s=0$, the output impedance of this case is similar to the output impedance of simple FVF (Eq. (13)).

The output impedance of the proposed FVF with a series combination of a resistor and an inductor ($Z=R+sL$) in the feedback path is given by

$$Z_{OUT} = \frac{1}{g_{m1}g_{m2}r_o(1 + (R + sL/R_b))} \tag{36}$$

At $s=0$, the output impedance of the proposed FVF depends upon the value of resistor (R). The comparison between Eqs. (13) and (36) shows, that the proposed FVF has lower output impedance than the conventional FVF. This decrement in the output impedance at high frequency is limited by the peaking in the frequency response and hence the value of Z cannot be chosen arbitrarily.

4. Application of the proposed FVF in a current mirror

The FVF is not new in the electronics world. It has been used in many circuits, such as current mirror (CM), level shifter, arithmetic circuits, current sensors etc. The demand of high speed analog and mixed signal circuits has influenced the work to propose a large bandwidth FVF. The CM investigated in [18] has utilized FVF in the input circuitry (Fig. 6). The proposed wideband FVF is applied in the current mirrors shown in Fig. 6 [18], Figs. 7 and 10 [28].

Gupta et al. have developed wideband low-voltage current mirrors (Figs. 7 and 10) in [28]. In this paper, the inductive-peaking technique is used to enhance the bandwidth of a FVF cell and the improved FVF cell is used in passively and actively compensated current mirrors (as shown in Figs. 8, 9 and 11).

5. Results and discussion

The proposed and conventional circuits are designed in TSMC 0.18 μm CMOS technology and simulated in Spectre simulator (Cadence), with supply voltage of 1.5 V. The circuit parameters of the FVF are given in Table 1.

The DC response of the FVF is shown in Fig. 12. Since at low frequency, there will be no current in the feedback path of the FVF, the linearity performance of the FVF is unaffected by the modification presented in the paper. The frequency responses of the conventional and proposed FVF cells are shown in Fig. 13. The frequency response depends on the value of the feedback element. The inductive-

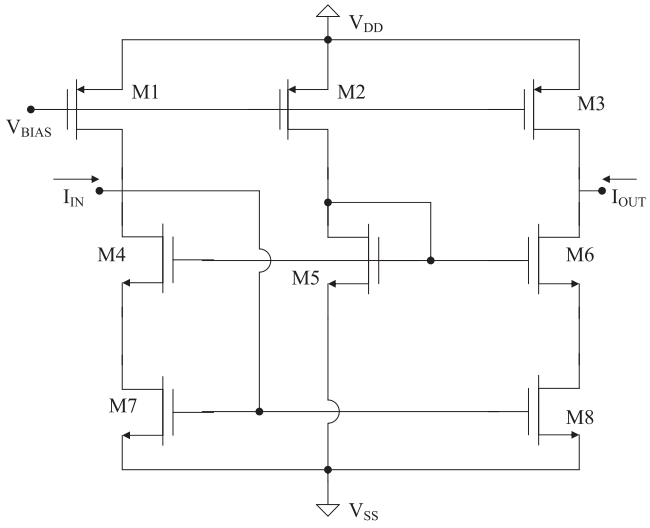

Fig. 6. Current mirror using conventional FVF [18].

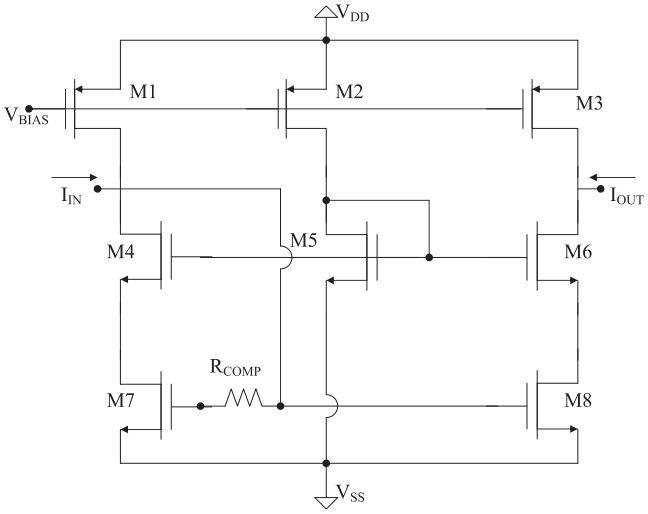

Fig. 7. Passively compensated current mirror [28].

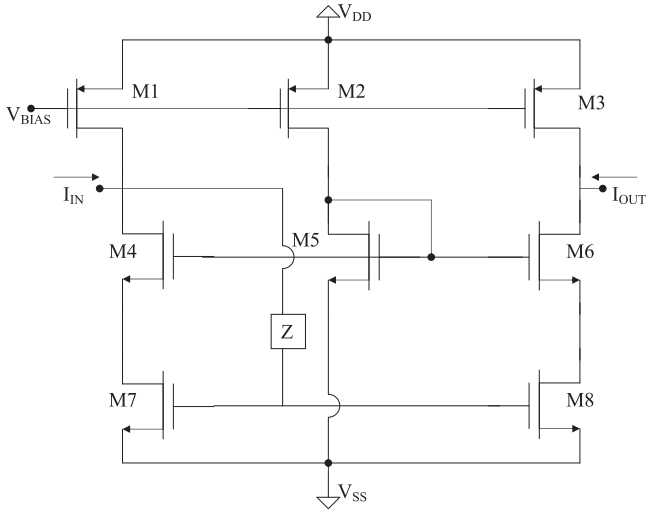

Fig. 8. Current mirror using proposed FVF.

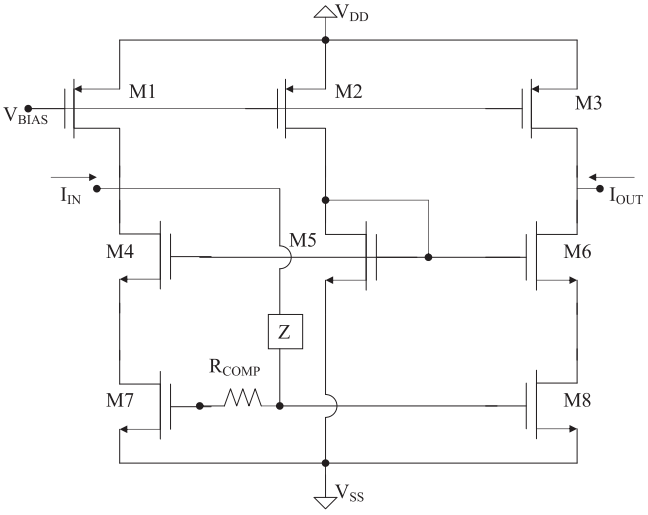

Fig. 9. Passively compensated current mirror using proposed FVF.

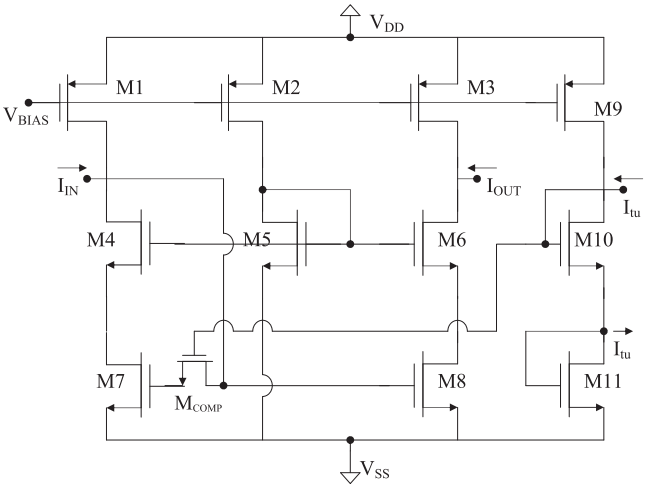

Fig. 10. Actively compensated current mirror [28].

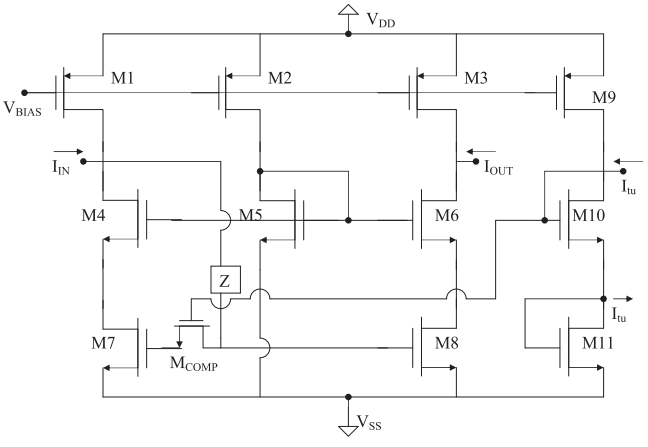

Fig. 11. Actively compensated current mirror using proposed FVF.

feedback FVF has BWER of 1.93 and 1.99 by using 0.5 μH and 5 nH, respectively. In the second case, where the feedback element is a series combination of a resistor ($R=10$ kΩ) and an inductor (sL), the proposed FVF has achieved BWER of 2.20 and 2.26 by using 0.5 μH and 5 nH, respectively. Since, inductor of value 0.5 μH cannot be easily implemented, therefore for the simulations of circuits, we have chosen inductor $L=5$ nH. The simulation results of the FVF cells are summarized in Table 2. The Monte Carlo simulation of the proposed FVF with

Table 1
Circuit parameters of FVF cell.

Circuit parameter	Value
Technology	180 nm
Power supply	1.5 V
DC bias current (I_b)	10 μA
Aspect ratio of M1	10
Aspect ratio of M2	20
Inductor L (in feedback path)	5 nH
Resistor R (in feedback path)	10 kΩ

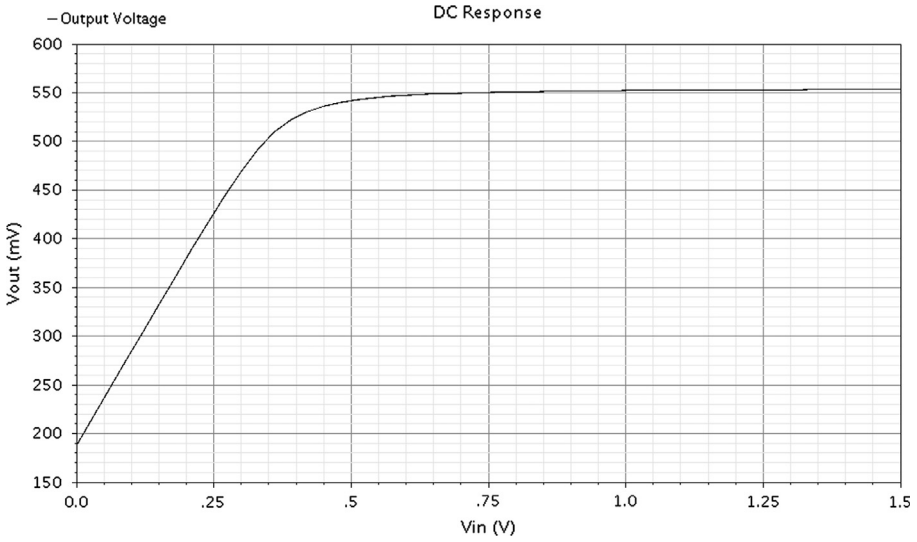

Fig. 12. DC responses of FVF cells.

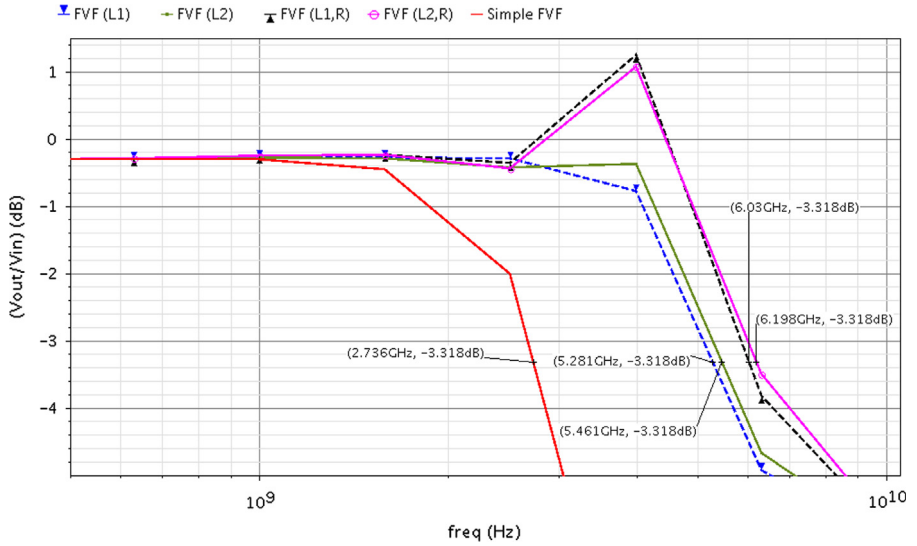

Fig. 13. Frequency responses of FVF cells ($L1=0.5$ uH, $L2=5$ nH and $R=10$ k).

inductor ($L=5$ nH) in the feedback path results into mean deviation of $-596.63e-12$ and standard deviation of $12.516e-9$. The FVF with series combination of a resistor ($R=10$ kΩ) and an inductor ($L=5$ nH) has shown mean deviation of $-632.47e-12$ and standard deviation of $12.941e-9$ in the Monte Carlo simulation by using Pspice (OrCAD).

The DC power dissipation (Fig. 14) of the proposed FVF is 5.564 μW, while the output impedance of the FVF is 173.7 Ω. From Fig. 15, it can be noticed that, the output impedance of the proposed FVF decreases faster than that of conventional FVF, at high frequency. This results into larger current at the output node. Thus justifies the approach of bandwidth extension, by using an impedance element in the feedback path of the FVF. The step response of the proposed and conventional FVF is shown in Fig. 16 and it can be noticed that, the

Table 2
The comparative results of the conventional and proposed FVF circuits.

Flipped voltage follower (FVF)			
Simulated circuit	**Conventional**	**FVF (L=5 nH)**	**FVF (L=5 nH and R=10 kΩ)**
Bandwidth (GHz) (simulation)	2.736	5.461	6.198
Bandwidth (GHz) (theoretical)	2.802	5.598	6.406
Error (%)	2.41	2.45	3.24
Noise at 100 kHz $(V^2/Hz) \times 10^{-15}$	1.23	1.25	1.42

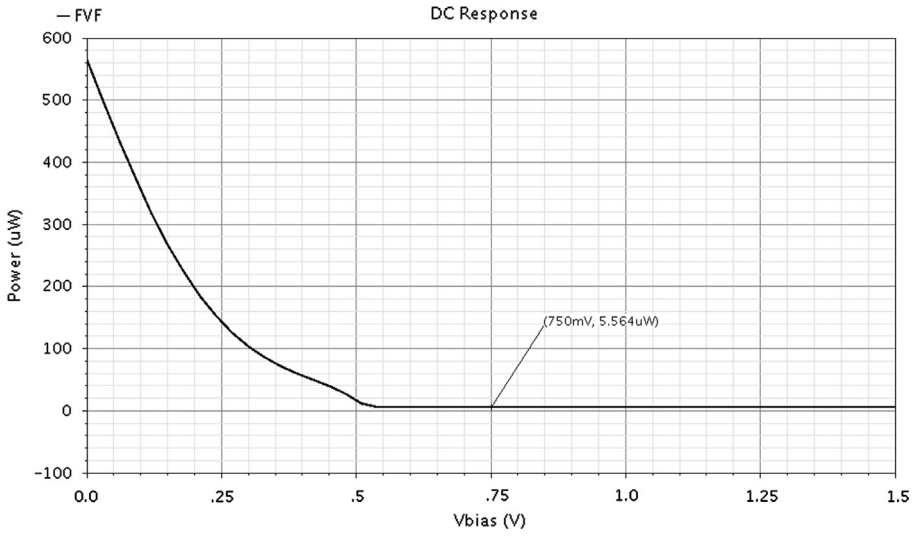

Fig. 14. DC power dissipation of FVF cell.

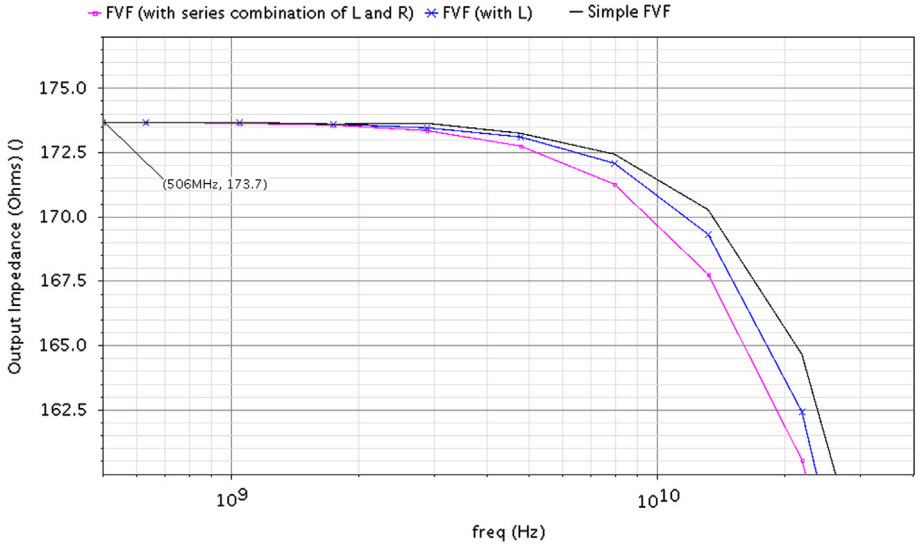

Fig. 15. Variations of output impedance with frequency of conventional FVF and proposed FVF.

rise-time of the proposed FVF is reduced as compared to the conventional FVF. Figs. 17–21 are the step responses of the FVF, by considering the effects of variations in width of M1, width of M2, power supply, bias current and temperature, respectively.

On simulating the current mirrors given in [18] with inductive-feedback FVF cell, the obtained BWER is 1.66 (i.e. an enhancement of 2.67 GHz). The proposed FVF cell provides BWER of 2.40 and 2.98 to passively compensated CM [28] without peaking and with peaking, respectively (Fig. 22). The frequency responses of actively compensated CM, with improved FVF cell are shown in Fig. 23 and have achieved BWER of 1.95 without peaking and 2.69 with peaking. The −3 dB frequencies of simulated current mirrors are given in Table 3. The comparative results of CM [18] and simulated CM are given in Table 4. The power supply voltage is 1.5 V and dc bias current is 50 μA.

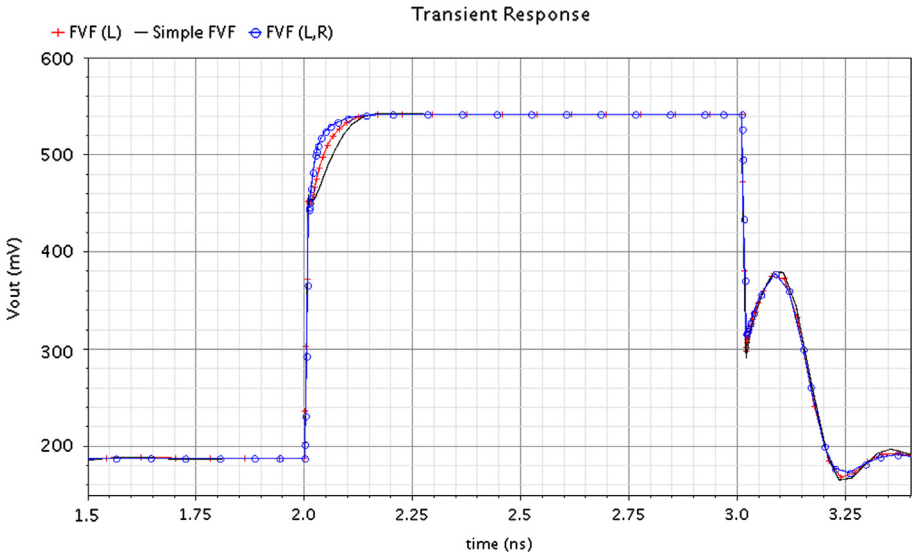

Fig. 16. Step responses of FVF cells.

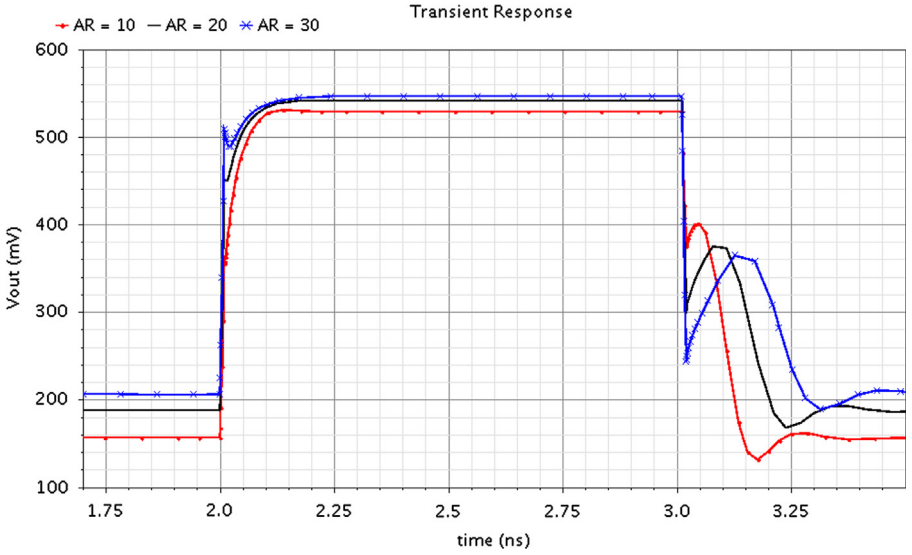

Fig. 17. Step response of proposed FVF cell (inductor as feedback element, only) considering the effect of width variation of M1 (where, AR stands for aspect ratio).

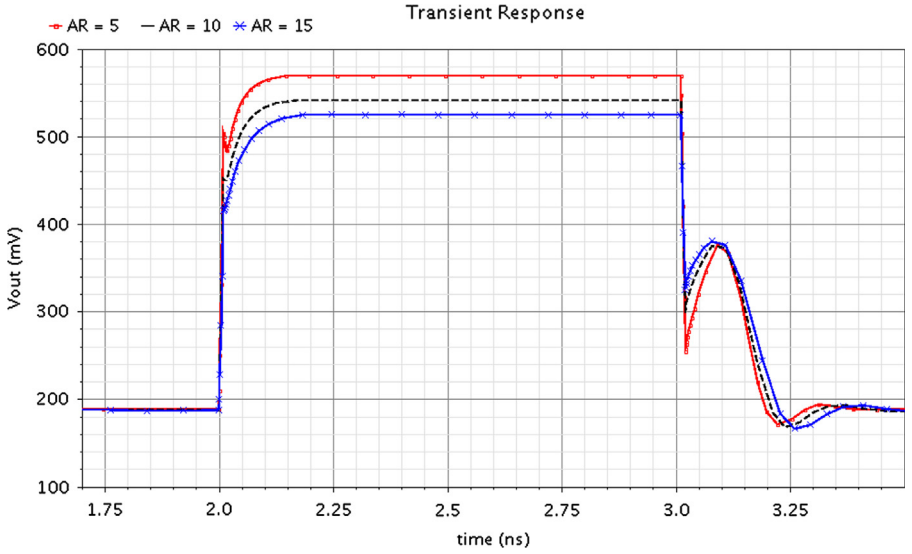

Fig. 18. Step response of proposed FVF cell (inductor as feedback element, only) considering the effect of width variation of M2 (where, AR stands for aspect ratio).

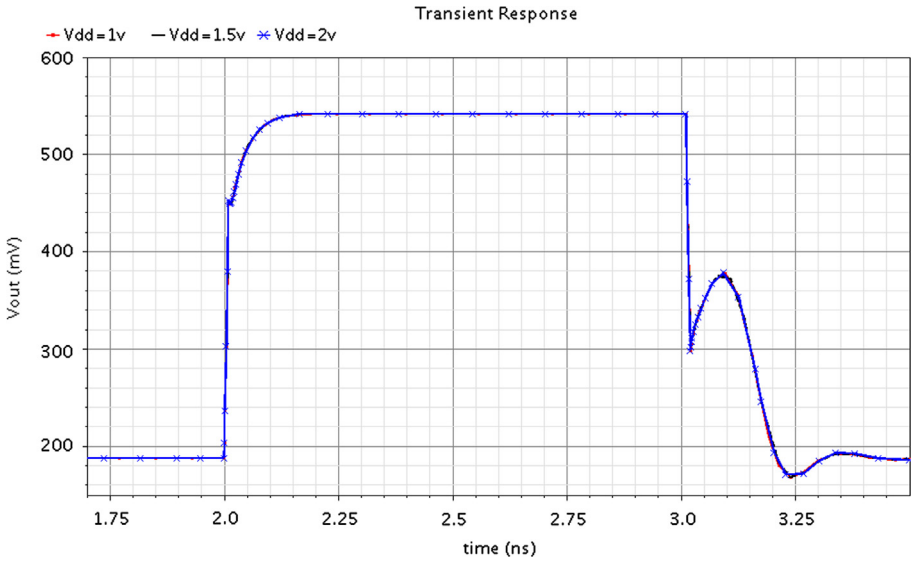

Fig. 19. Step response of proposed FVF cell (inductor as feedback element, only) considering the effect of power supply variation.

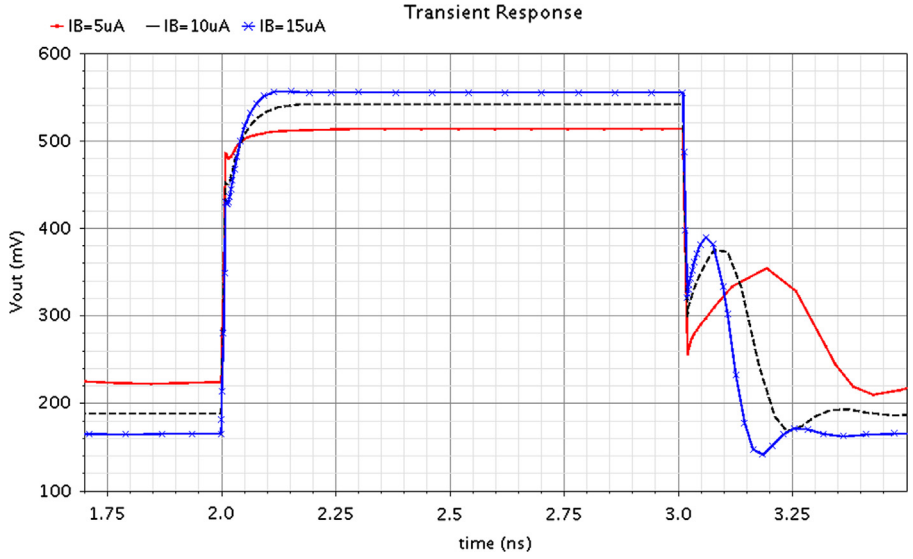

Fig. 20. Step response of proposed FVF cell (inductor as feedback element, only) considering the effect of bias current variation.

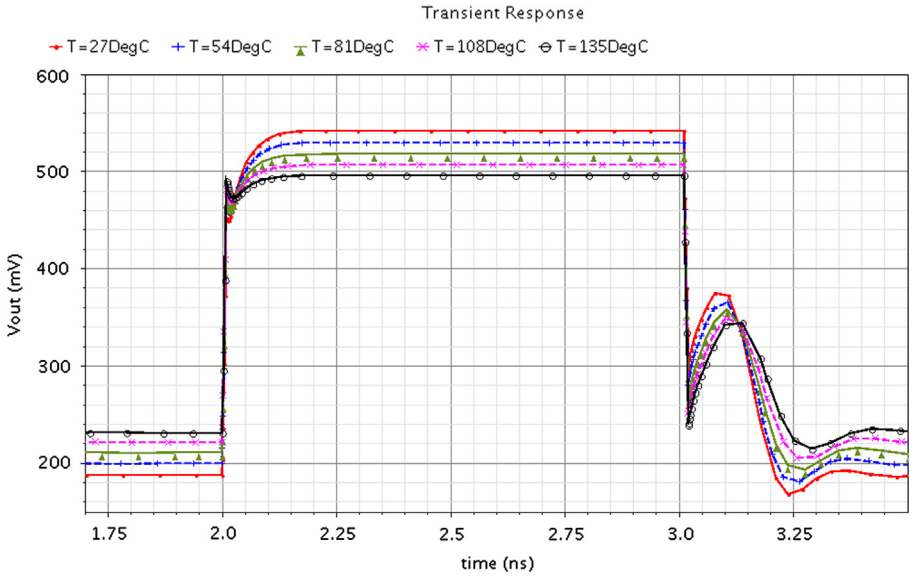

Fig. 21. Step response of proposed FVF cell (inductor as feedback element, only) considering the effect of temperature variation.

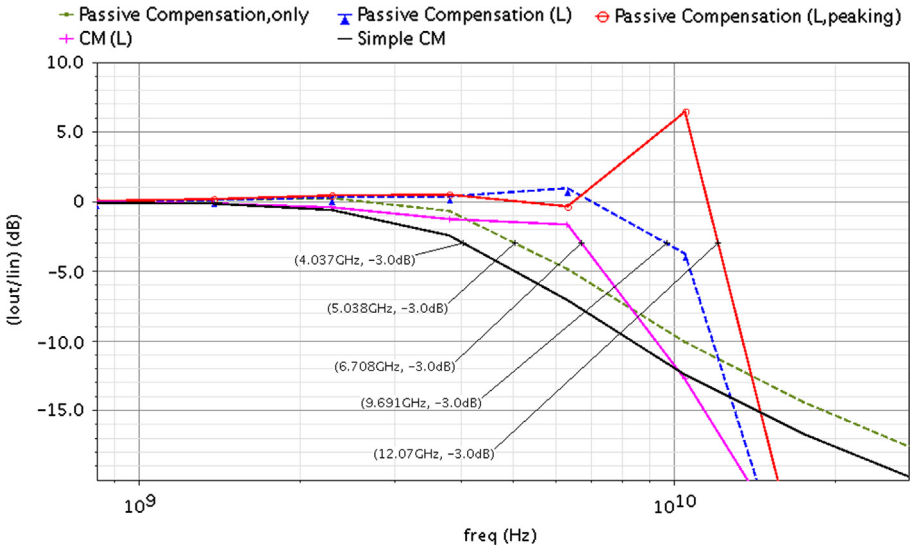

Fig. 22. Frequency responses of current mirrors (shown in Figs. 6–9, where '*L*, peaking' is a series combination of *L* & *R*).

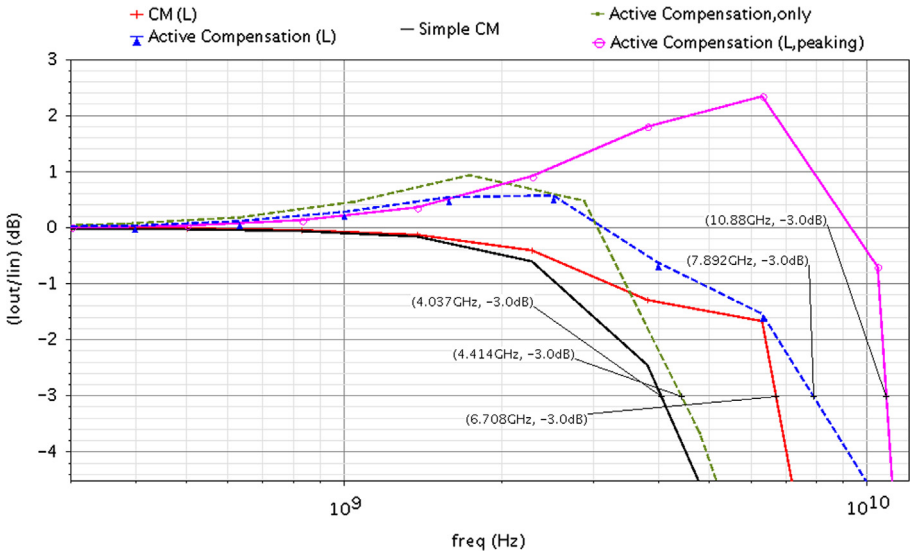

Fig. 23. Frequency responses of current mirrors (shown in Figs. 6,8,10 and 11, where '*L*, peaking' is a series combination of *L* & *R*).

Table 3
−3 dB frequency of simulated current mirrors.

Simulated circuits	−3 dB frequency (GHz)
Current mirror (CM)	4.037
Passively compensated CM	5.038
CM (feedback element is *L*)	6.708
Passively compensated CM (with *L*)	9.691
Passively compensated CM (with *L*, peaking)	12.07
Actively compensated CM	4.414
Actively compensated CM (with *L*)	7.892
Actively compensated CM (with *L*, peaking)	10.88

The current transfer error ($I_{out}-I_{in}$) of the CM is shown in Fig. 24 and it is about −3.37%. The input and output compliances are shown in Figs. 25 and 26, respectively. The DC power dissipation of the CM (Fig. 27) is 324.3 μW. It can be observed that, the DC performance factors are invariant by the modification in the CM. The variation of input and output impedances with frequency of the CM (shown in Figs. 28 and 29) are 1.935 kΩ and 0.22 MΩ, respectively. The output impedance remains same for the conventional and proposed CM.

Table 4
Comparison results of current mirror (Fig. 6).

Performance factor	Current mirror [18]	Simulated current mirror
Aspect ratio	5.45	20
dc power dissipation (μW)	218	324.3
Input resistance (kΩ)	3	1.93
Current transfer error (%)	1.4	−3.37
cut-off frequency	212 MHz	4.037 GHz (without L) and 6.708 GHz (with L)

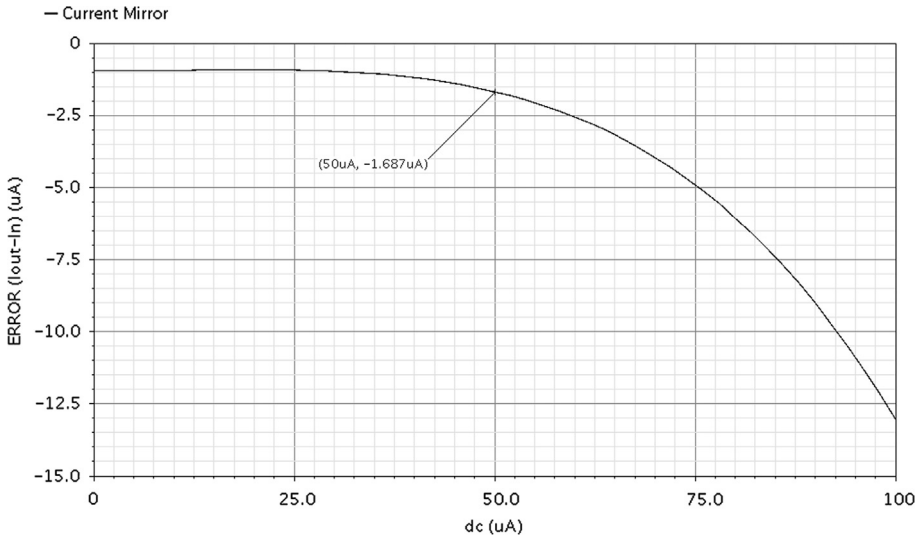

Fig. 24. Current transfer error (I_{out}–I_{in}) of current mirror.

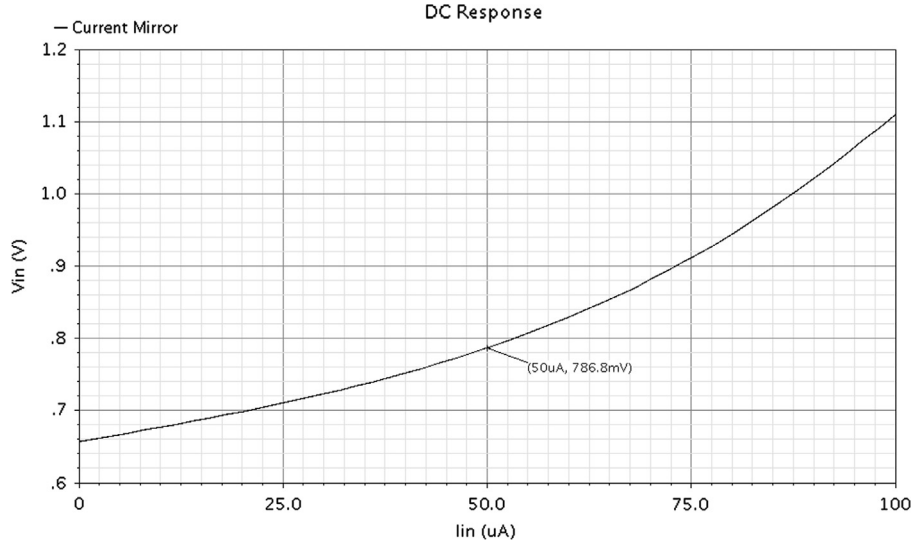

Fig. 25. Input voltage (V_{in}) as a function of input current (I_{in}) of current mirror.

It can be seen from frequency responses of the simulated circuits, that the gain of the systems are unaffected by using inductive-peaking bandwidth extension technique in the conventional FVF.

6. Conclusion

A high frequency FVF based on inductive-peaking technique has been proposed in the paper. The newly developed FVF accounts for very large bandwidth and low output impedance at high frequency, without extra DC power dissipation. It is shown in the work that by employing an inductive-element in the feedback path, the new FVF has achieved 1.99 BWER, without affecting the mid-band gain of the voltage follower and

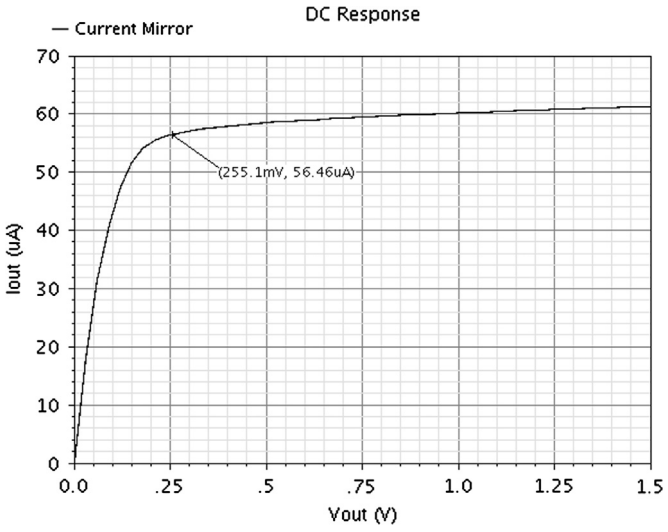

Fig. 26. Output current (I_{out}) versus output voltage (V_{out}) of current mirror.

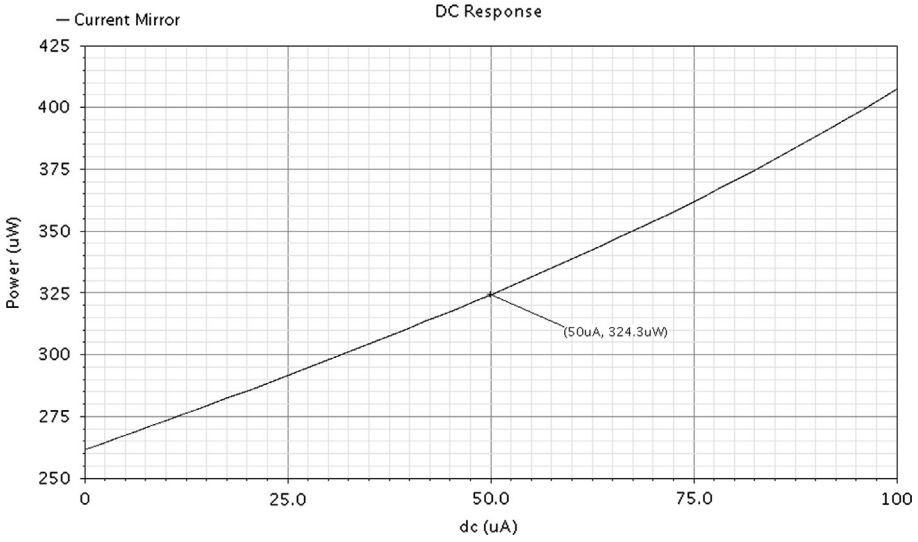

Fig. 27. DC power dissipation of current mirror.

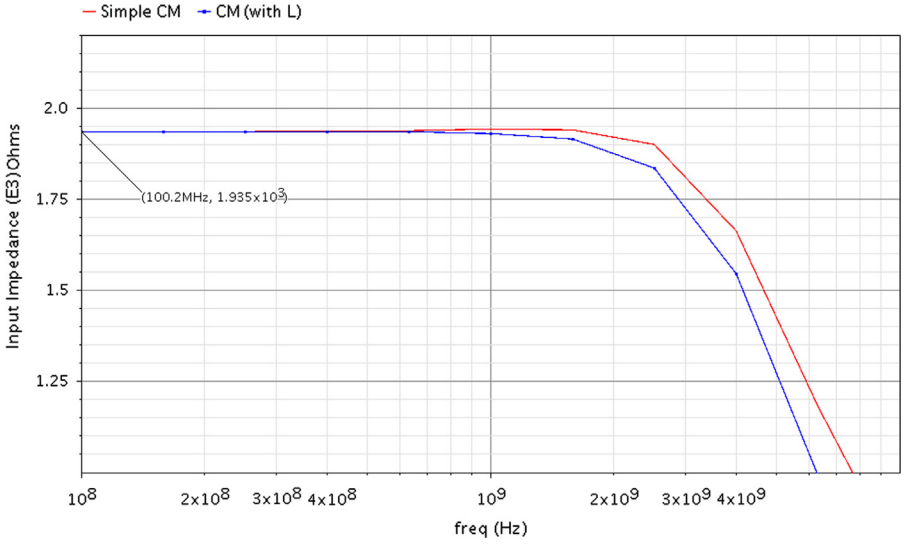

Fig. 28. Input impedance variation with frequency of current mirror.

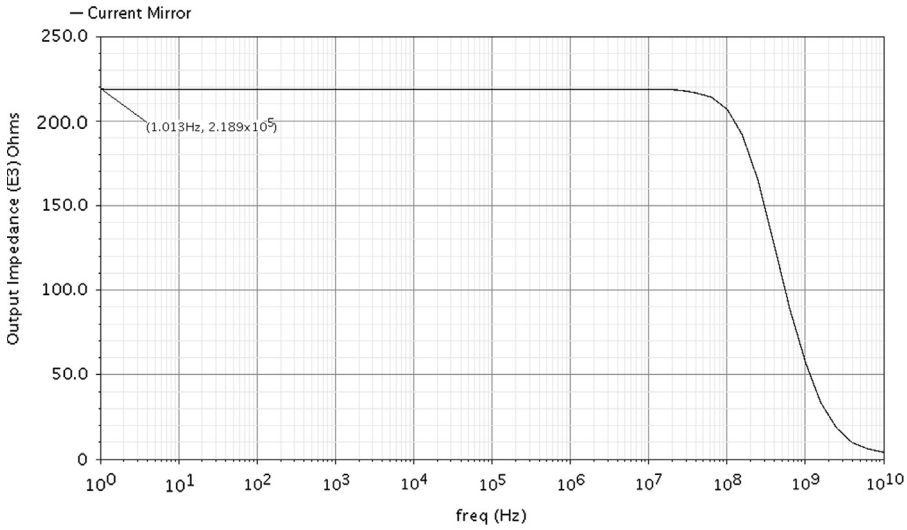

Fig. 29. Output impedance variation with frequency of current mirror.

Table 5
Routh array of the proposed FVF (Eq. (18)).

s^3	$r_o{}^2C_{gs}{}^2L(R_b+r_o)$	$r_o{}^2C_{gs}\{r_o+3R_b+g_{m1}r_oR_b\}$
s^2	$r_oC_{gs}\{r_o{}^2C_{gs}R_b+L(2r_o+R_b)+g_{m1}r_o{}^2L\}$	$g_{m1}g_{m2}r_o{}^3R_b$
s^1	$\left(\frac{g_{m2}C_{gs}{}^2r_o{}^3R_b{}^2}{C_{gs}R_b+g_{m1}L}\right)$	0
s^0	$g_{m1}g_{m2}r_o{}^3R_b$	0

Table 6
Routh array of the proposed FVF (Eq. (26)).

s^3	$r_o{}^2C_{gs}{}^2L(R_b+r_o)$	$r_oC_{gs}\{r_o(R_b+r_o)+R_bR+g_{m2}r_o{}^2(R+R_b)\}$
s^2	$r_oC_{gs}\{r_oC_{gs}(R(R_b+r_o)+R_br_o)+LR_b+g_{m1}r_o{}^2L\}$	$g_{m1}g_{m2}r_o{}^3R_b$
s^1	$\left(\frac{g_{m2}C_{gs}r_o{}^3(C_{gs}R_b(R+R_b)+g_{m1}LR)}{C_{gs}(R+R_b)+g_{m1}L}\right)$	0
s^0	$g_{m1}g_{m2}r_o{}^3R_b$	0

thus it is more suitable to be used in high speed devices than the conventional FVF. The trend obtained for the output impedance with frequency has proved that, the proposed FVF cells can be preferred over a conventional FVF in high-speed applications. The described circuit-level implementation of the proposed model of FVF can be used in different analog and mixed-signal circuits and in the work it has been shown to be useful in current mirror.

References

[1] N. Charalampidis, K. Hayatleh, B.L. Hart, F.J. Lidgey, A. High, Frequency low distortion voltage- follower, IEEE International Conference on Circuits and Systems Poceedings (2006) 2291–2294.
[2] R.G. Carvajal, J. Ramirez-Angulo, A. Lopez Martin, A. Torralba, J. Galan, et al., The flipped voltage follower: a useful cell for low voltage low power circuit design, IEEE Transactions on Circuits and Systems I 52 (7) (2005) 1276–1279, http://dx.doi.org/10.1109/TCSI.2005.851387.
[3] Chaiwat Sakul, Kobchai Dejhan, Squaring and square-root circuits based on flipped voltage follower and applications, International Journal of Information Systems and Telecommunication Engineering 1 (2010) 19–24.
[4] R.G. JRamirez-Angulo, Carvajal A. Torralba, J. Galan, A.P. Vega-Leal, et al., Low-power low-voltage analog electronic circuits using the flipped voltage follower, IEEE International Conference on Industrial Electronics 4 (2002) 1327–1330.
[5] S. Javad Azhari, H. Faraji Baghtash, K. Monfaredi, A novel-ultra high compliance, high output impedance low power very accurate high performance current mirror, Microelectronics Journal 42 (2) (2011) 432–439.
[6] Hugues J. Achigui, Christian Fayomi, Daniel Massicotte, Mounir Boukadoum, Low-voltage, high-speed CMOS analog latched voltage comparator using the “flipped voltage follower” as input stage, Microelectronics Journal 42 (2011) 785–789.
[7] Tamer Farouk, Ahmed N. Mohieldin, Ahmed H. Khalil, A low-voltage low-power CMOS fully differential linear transconductor with mobility reduction compensation, Microelectronics Journal 43 (2012) 69–76.
[8] S. Lai, H. Zhang, G. Chen, J. Xu, An improved source follower with wide swing and low output impedance, IEEE Asia Pacific Conference on Circuits and Systems (2008) 814–818.
[9] J. Ramirez-Angulo, Sheetal Gupta Ivan Padilla, R.G. Carvajal, A. Torralba, M. Jime´nez, et al., Comparison of conventional and new flipped voltage structures with increased input/output signal swing & current sourcing/sinking capabilities, IEEE 48th Midwest Symposium on Circuits and Systems 2 (2005) 1151–1154.
[10] Yasutaka Haga, Izzet Kale, Bulk-driven flipped voltage follower, IEEE International Symposium on Circuits and Systems (2009) 2717–2720.
[11] T. Voo, C. Toumazou, High-speed current mirror resistive compensation technique, IEE Electronics Letters 31 (4) (1995) 248–250.
[12] D.J. Comer, D.T. Comer, J.B. Perkins, K.D. Clark, A.P.C. Genz, Bandwidth extension of high-gain CMOS stages using active negative capacitance, IEEE Transactions on Circuits and Systems (2006) 628–631.
[13] Willy Sansen, Z.Y. Chang, Feedforward compensation techniques for high-frequency CMOS amplifiers, IEEE Journal of Solid-State Circuits 25 (6) (1990) 1590–1595.

[14] S. Shekhar, J.S. Walling, David J. Allstot, Bandwidth extension techniques for CMOS amplifiers, IEEE Journal of Solid State Circuits 41 (11) (2006) 2424–2439.
[15] L. Bouzerara, M.T. Belaroussi, B. Amirouche, Low-voltage, low-power & high gain CMOS OTA using active positive feedback with feedforward & FDCM technique, IEEE 23rd International Conference on Microelectronics 2 (2002) 573–576.
[16] Sunderarajan S. Mohan, Mariadel Mar Hershenson, Stephen P. Boyd, Thomas H. Lee, Bandwidth extension in CMOS with optimized on-chip inductors, IEEE Journal of Solid-State Circuits 35 (3) (2000) 346–355.
[17] Bendong Sun, Fei Yuan, Ajoy Opal, A new differential CMOS current-mode preamplifier for GBps data communications, Analog Integrated Circuits and Signal Processing 44 (2005) 191–201.
[18] C. Koliopoulos, C. Psychalinos, A comparative study of the performance of the flipped voltage follower based low voltage current mirror, IEEE International Symposium on Signals, Circuits and Systems 1 (2007) 1–4, http://dx.doi.org/10.1109/ISSCS.2007.4292650.
[19] Adel S. Sedra, Kenneth C. Smith, Microelectronics Circuits, fifth ed., Oxford University Press, New York, 2005.
[20] Thomas H. Lee, The design of CMOS radio-frequency integrated circuits, second ed., Cambridge University Press, U.K., 2004.
[21] Mahdi Ebrahimzadeh, A low voltage, high quality factor floating gate tunable active inductor with independent inductance and quality factor tuning, International Journal of Computer and Electrical Engineering 3 (2) (2011) 180–183.
[22] R.B. Merrill et al., Optimization of high Q integrated inductors for multilevel metal CMOS, in: Proceedings of the IEDM Technical Digest, 1995.
[23] J.N. Burghartz, et al., Multilevel-spiral inductors using VLSI interconnect technology, IEEE Electron Device Letters 17 (1996) 428–430.
[24] Chao-Chih Hsiao, Chin-Wei Kuo, Chien-Chih Ho, Yi-Jen Chan, Improved quality-factor of 0.18-um CMOS active inductor by a feedback resistance design, IEEE Microwave and Wireless Components Letters 12 (12) (2002) 467–469.
[25] C. Li, F. Gong, P. Wang, Analysis and design of a high-Q differential active inductor with wide tuning range, IET Circuits, Devices and Systems 4 (6) (2010) 486–495.
[26] Abu Khari Chun-Lee Ler, Bin A′ain, Albert Victor Kordesch, CMOS active inductor linearity improvement using feed-forward current source technique, IEEE Transactions on Microwave Theory and Techniques 57 (8) (2009) 1915–1925.
[27] J.V.D. Vegte, Feedback Control Systems, 2nd ed., Prentice Hall, Englewood Cliffs, NJ, 1990.
[28] Maneesha Gupta, Prashant Aggarwal, Pritender Singh, Naveen Kumar Jindal, Low voltage current mirrors with enhanced bandwidth, Analog Integrated Circuit Signal Process 59 (1) (2009) 97–103, http://dx.doi.org/10.1007/s10470-008-9241-2.